Journal of Materials Chemistry

Cite this: J. Mater. Chem., 2011, 21, 18810

www.rsc.org/materials

PAPER

Synthesis of 1D and heavily doped $Zn_{1-x}Co_xO$ six-prism nanorods: improvement of blue–green emission and room temperature ferromagnetism

Tao Wang,[a] Yanmei Liu,*[a] Yangguang Xu,[c] Gang He,[a] Guang Li,[a] Jianguo Lv,[a] Mingzai Wu,[ab] Zhaoqi Sun,[a] Qingqing Fang,[a] Yongqing Ma[a] and Junlei Li[a]

Received 14th June 2011, Accepted 22nd September 2011
DOI: 10.1039/c1jm12721g

In this work, one-dimensional (1D) and heavily doped $Zn_{1-x}Co_xO$ ($x = 0.05$, 0.1, 0.15 and 0.2) nanorods (NRs) were successfully fabricated by a new solvothermal method. Such a $Zn_{1-x}Co_xO$ nanorod exhibits a hexagonal prism-like microcrystal with a pyramidal top. Analyses from transmission electron microscopy (TEM) and high-resolution transmission electron microscopy (HRTEM) indicated that $Zn_{1-x}Co_xO$ NRs possess perfect single crystal wurtzite structures. The influence of Co doping on the structural, optical and magnetic properties of NRs was investigated in detail. It was verified that Co was successfully doped into the ZnO wurtzite lattice structure by X-ray diffraction (XRD) and energy-dispersive spectroscopy (EDS). The $Zn_{1-x}Co_xO$ NRs show an obvious blue–green emission except for the weak UV emission. The corresponding luminescence mechanism was discussed, and the environment of cobalt in the ZnO wurtzite lattice was also identified through UV-vis spectroscopy. In addition, the magnetic hysteresis (M–H) curves demonstrated that the $Zn_{1-x}Co_xO$ NRs possess obvious ferromagnetic characteristics at room temperature. These $Zn_{1-x}Co_xO$ NRs are suggested to have potential applications in spintronic, field emission and optoelectronic devices, *etc*.

Introduction

The use of intentional impurities or dopants to control the behavior of materials has been at the heart of many technologies.[1] However, doping has proven elusive for strongly confined colloidal semiconductor nanocrystals because of the synthetic challenge of how to introduce single impurities, as well as a lack of fundamental understanding of this heavily doped limit under strong quantum confinement.[2] Therefore, improving synthetic control over dopant incorporation, optimizing their concentrations, and investigating the phenomena that emerge will be an exciting and challenging task.[1]

ZnO-based nanomaterials have attracted considerable attention in the research community for their potential high technology applications because of their wide band gap ($E_g = 3.37$ eV), excellent chemical and thermal stability, specific electrical and optoelectronic properties, and large exciton binding energy.[3] Among the reported ZnO-based nanomaterials, transition-metal (TM) doped ZnO are very important for their pronounced optical and electronic properties and controllable magnetic properties at room temperature.[4–6] They are expected to be significant in diluted magnetic semiconductors (DMSs) and have potential applications in spintronics and optoelectronics. So far considerable efforts have been made for the synthesis of 1D and TM doped ZnO nanomaterials.[7–10] However, because the increasing impurities in the host lattice are blocked by a growing surface energy and lattice distortion, the growth of the 1D structure is usually hindered in the heavy doping system. So synthesis of doped ZnO nanorods with narrow size distribution and high crystallinity still remains a significant challenge.[11]

In this study, we report the fabrication of 1D $Zn_{1-x}Co_xO$ ($x = 0.05$, 0.1, 0.15 and 0.2) six-prism NRs by a facile solvothermal method. Characterization results demonstrated that $Zn_{1-x}Co_xO$ NRs exhibit an enhanced blue–green emission and room temperature ferromagnetism. The structural, optical and magnetic properties induced by cobalt doping of ZnO were also studied. The HRTEM characterization confirmed that the NRs possess a perfect single crystal wurtzite structure. Co was successfully doped into the lattice of ZnO as revealed by XRD and verified by the analysis of XPS and EDX. The results of UV-vis spectroscopy further indicated that tetrahedrally coordinated Co^{2+} ions substitute for Zn^{2+} in the hexagonal ZnO wurtzite structure. Besides, taken together with previous reports, we consider that the surface defect plays a vital role on the visible

[a]*Anhui Provincial Key Laboratory of Information Materials and Devices, Anhui University, Hefei, 230039, People's Republic of China. E-mail: wang_shu_guang@163.com; lymwt2009@163.com*
[b]*Key Laboratory of Materials Physics, Institute of Solid State Physics, Chinese Academy of Sciences, Hefei, 230031, People's Republic of China*
[c]*CAS Key Laboratory of Mechanical Behavior and Design of Materials, Department of Modern Mechanics, University of Science and Technology of China (USTC), Hefei, 230027, People's Republic of China.*

emission. The results from these studies aid in the understanding of the relationship between morphology, structure, and optical properties, which is helpful for the application in devices.

Experimental section

All chemicals were analytical grade and purchased from Jin Chang New Material Corp. A detailed flowchart which shows the experimental procedure used for preparing $Zn_{1-x}Co_xO$ NRs is given in Fig. 1. Firstly, the precursor solution consists of 0.05 M zinc acetate dihydrate ($Zn(Ac)_2 \cdot 2H_2O$) and 0.035 M sodium hydroxide (NaOH) and different contents of cobalt nitrate hexahydrate ($Co(NO_3)_2 \cdot 6H_2O$) dissolved in 2-methoxyethanol. 0.05 M of monoethanolamine (MEA) was then added to the mixture, which was stirred at 90 °C for 10 min until a milky and saturated liquid appeared, and then cooled naturally to room temperature. 20 mL ammonium hydroxide was added to the mixture and stirring continued for 10 min at room temperature. Finally, the mixture was added into a Teflon-lined stainless steel autoclave, sealed and maintained at 180 °C for 10 h. After the autoclave was cooled naturally to room temperature, the obtained precipitate was washed with deionized water followed by ethanol to remove ions possibly remaining in the final product, and then dried at 80 °C in air for further characterization.

The phase purity and crystal structure of the samples were analyzed by XRD (MAP18AHF) by using CuKα radiation (λ = 1.54 Å) at the excitation voltage of 40 kV and a tube current of 100 mA. The morphology and composition of the samples were examined by a Sirion200 scanning electron microscope (SEM) combined with EDS. TEM images and selected area diffraction patterns (SAED) were obtained by TEM. Fourier transform infrared (FTIR) spectra were measured on a NEXUS-870 FTIR system using KBr pellets. Photoluminescence (PL) spectra were taken at room temperature following excitation with a Xenon lamp laser (λ = 325 nm). In order to investigate the optical absorbent properties of the samples, thin slices prepared from $Zn_{1-x}Co_xO$ powder was first prepared, pure barium sulfate ($BaSO_4$) was used as calibrating reference, and then the UV-vis adsorption data was obtained by using a U-4100 spectrophotometer. Magnetic hysteresis loops were measured by a vibrating sample magnetometer (VSM, BHV-55) at room temperature.

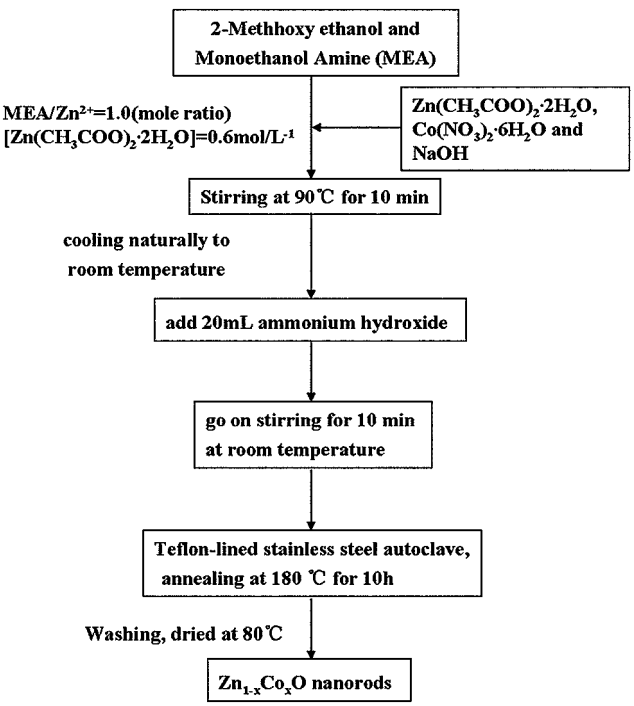

Fig. 1 Schematic illustration of the procedure for preparing $Zn_{1-x}Co_xO$ NRs.

Results and discussion

The main purpose of the current work is to propose a new synthetic method to prepare heavily doped $Zn_{1-x}Co_xO$ NRs and investigate their morphology and structural, optical and magnetic properties. Generally speaking, the solubility of transition metals in ZnO is limited. Among transition metals, Co and Mn have been reported and proven to be the most soluble in ZnO.[12] Under non-equilibrium conditions (such as the pulsed laser deposition), a solubility of 33% Co in ZnO has been achieved.[13] However, it is much lower in the low-temperature synthesis procedure.[14] Viswanatha *et al.*[15] reported that the

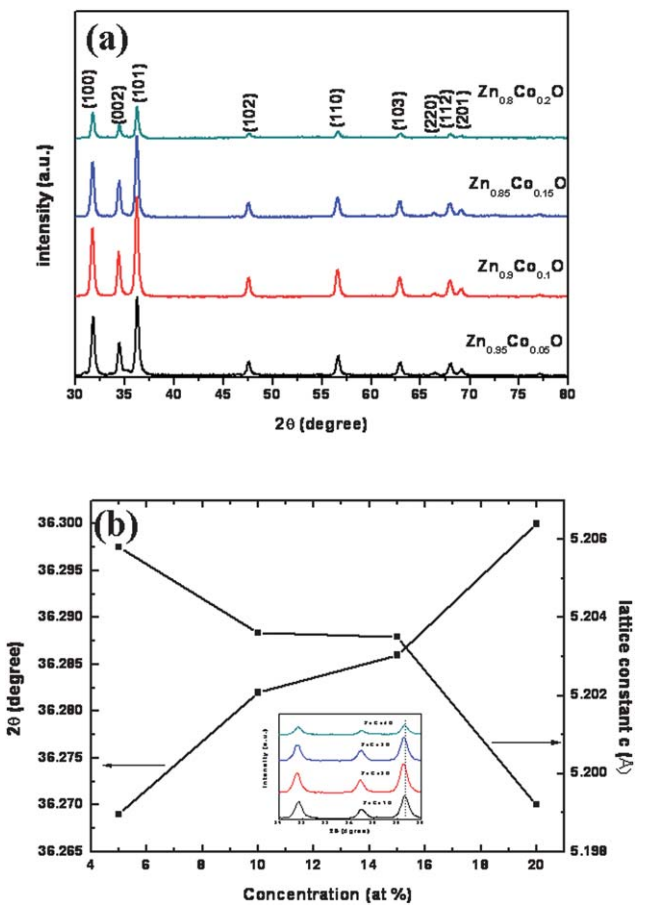

Fig. 2 (a) XRD patterns taken from the $Zn_{1-x}Co_xO$ NRs. (b) Variation in the (101) peak position and *c*-axis parameter with the concentration of Co^{2+}. Inset of (b), the XRD pattern of the three most intense peaks [(100), (002), and (101)] for the $Zn_{1-x}Co_xO$ NRs.

solubility limit drastically reduced to as low as ~1% for the Mn-doped ZnO nanocrystals. But it is noteworthy mentioning that the solvothermal method can effectively improve the solubility of Co and Mn in ZnO; Wang *et al.*[16] reported that the solubility of Co in ZnO nanostructures is close to 15 at.%. Here, in our low-temperature system, the measured solubility of Co in ZnO, ranging from 3 to 18.45%, has been reached by the scope of heavy doping.

Typical XRD patterns of $Zn_{1-x}Co_xO$ ($x = 0.05$, 0.1, 0.15 and 0.2) NRs are presented in Fig. 2a. All the diffraction peaks can be indexed to the ZnO wurtzite structure (space group $P6_3mc$). No additional reflections are observed even for the samples with the largest amount of dopant, indicating that there are no additional crystalline structures present in the samples. Besides, it should be noted that the three most intense peaks of the XRD pattern of $Zn_{1-x}Co_xO$ nanostructures appear distinctly deteriorated when $x \geq 0.1$, which may suggest that heavy doping has a serious influence on the crystallization of ZnO. Fig. 2b clearly shows that the (101) peaks of all samples shift towards higher angles and the *c*-axis parameter decreases obviously with the increase in Co^{2+} content. The results may be induced by Co^{2+} substitution in ZnO lattices, causing a reduction of the unit cell. This is consistent with the fact that the ionic radius of Co^{2+} is 0.72 Å, whereas that of Zn^{2+} is 0.74 Å.[17]

Fig. 3a shows a representative SEM image of as-synthesized $Zn_{0.95}Co_{0.05}O$ NRs. It can be seen that the sample exhibits a hexagonal prism-like microcrystal with a pyramidal top, the length of which is about 3–4 μm and the diameter is ~200 nm. Inset of Fig. 3a is the high magnification view of the nanorod, and the detailed morphology is visible. This moderately long and perfectly straight nanorod is ideal for applications in field emission and electron spin. We also performed a detailed TEM study on the $Zn_{1-x}Co_xO$ nanostructures with a JEM-2100 TEM operated at 200 kV. TEM images of $Zn_{1-x}Co_xO$ NRs are shown in Fig. 3b–3g, which verify the observed morphology of $Zn_{1-x}Co_xO$ samples by SEM.

In order to further determine the structure and composition of doped ZnO samples, HRTEM and SAED techniques were performed as well (Fig. 3h and 3j). The HRTEM image of a Co doped ZnO nanorod (Fig. 3h) exhibits clear lattice fringes, indicating a high crystallinity of the nanorod. The recognized lattice spacing of 0.26 nm may suggest that the growth direction of the hexagonal wurtzite ZnO is along [0001]. The SAED pattern obtained from a nanorod (Fig. 3j) displays well defined spots with the zone axis of [0001] parallel to the basal plane. It provides further confirmation that the rods grow along the [0001] direction.

To investigate the bonding characteristics and the chemical state of the Co dopants in the $Zn_{0.8}Co_{0.2}O$ sample, the Co 2p core-level XPS has been performed, as shown in Fig. 4a. There are four peaks in Fig. 4a: a Co $2p_{3/2}$ peak at 780.8 eV, a Co $2p_{1/2}$ peak at 796.7 eV and their corresponding shake-up satellites at slightly higher energies. The existence of shake-up satellites located at the higher binding energy position suggests that Co exists in the form of a +2 state within Co-doped ZnO nanorods, because it is well-known that divalent cobalt (CoO) normally exhibits a stronger satellite shake-up structure.[18,19] The high-spin divalent state of Co ($3d^7$; $S = 3/2$) in the sample is expected for substituted Co ions at the Zn sites.[20]

The compositional analyses by EDS were also carried out, and the existence of Co, Zn, O and C in the $Zn_{0.8}Co_{0.2}O$ sample has been confirmed (Fig. 4b). The element C is ascribed to the conductive adhesives on the stage. According to the observation from EDS, it can be concluded that Co has entered the ZnO

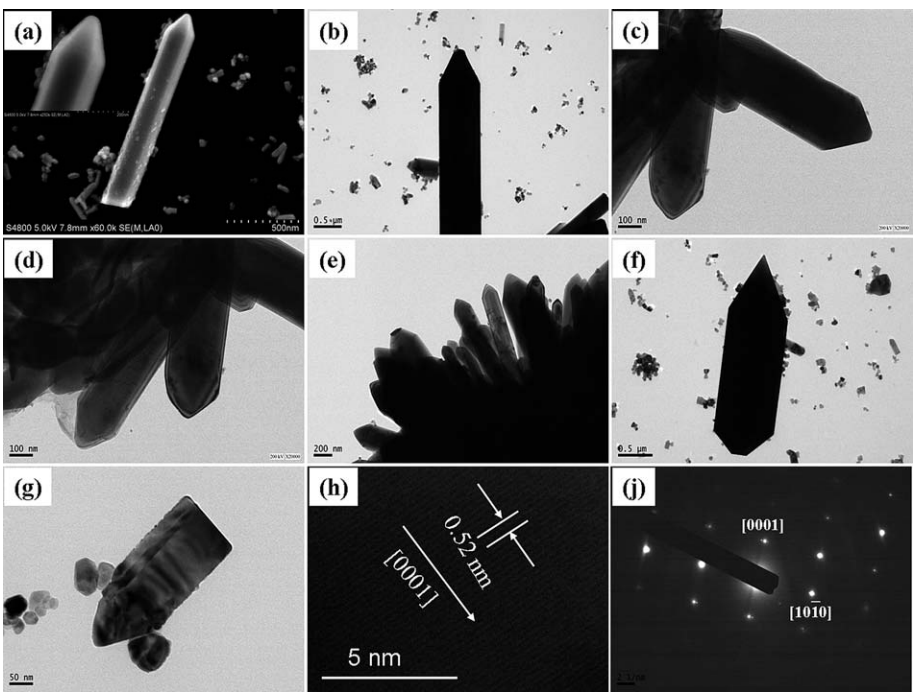

Fig. 3 (a): Representative SEM image of $Zn_{0.95}Co_{0.05}O$ nanorods; (b)-(g): Typical TEM images of $Zn_{1-x}Co_xO$ nanorods: (b) $Zn_{0.95}Co_{0.05}O$; (c)–(d): $Zn_{0.9}Co_{0.1}O$; (e): $Zn_{0.85}Co_{0.15}O$; (f)–(g) $Zn_{0.8}Co_{0.2}O$. (h) HRTEM image of $Zn_{0.85}Co_{0.15}O$ nanorods. (j) SAED pattern of $Zn_{0.85}Co_{0.15}O$ nanorods.

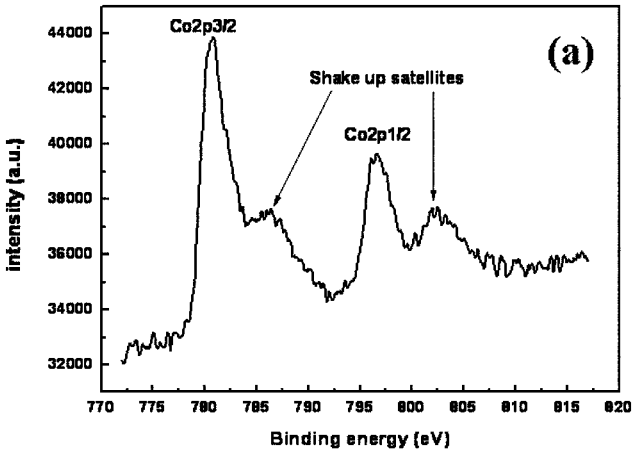

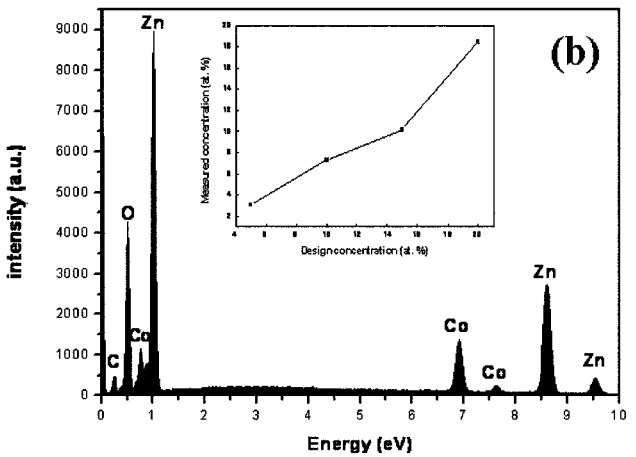

Fig. 4 (a): Co 2p XPS spectrum of $Zn_{0.8}Co_{0.2}O$ NRs; (b): the energy dispersive spectrum (EDS) of $Zn_{0.8}Co_{0.2}O$ NRs; inset of (b): the plot of measured concentration of Co against design concentration.

nanorod, and the estimated Co concentration in ZnO rods is 18.45 at.%, which is consistent with the 20 at.% initial concentration. The composition characterization of the other samples was also performed by EDS, and the inset of Fig. 4 offers the measured results, they are: 3 at.%, 7.31 at.%, 11.21 at.% and 18.45 at.% for $Zn_{0.95}Co_{0.05}O$, $Zn_{0.9}Co_{0.1}O$, $Zn_{0.85}Co_{0.15}O$ and $Zn_{0.8}Co_{0.2}O$, respectively.

The formation of the ZnO wurtzite structure was further supported by FTIR spectra (as shown in Fig. 5). All of the samples show similar spectra: absorption bands at ~470 cm^{-1} are assigned to the stretching vibrations of Zn–O; those at ~1380 and 1580 cm^{-1} are attributed to be the symmetric and asymmetric stretching vibrations of the carboxyl group ($-COO^-$), respectively; [21–23] those at ~3400 cm^{-1} represent the O–H mode, which may be due to the vibration of adsorbed water. These observations are in agreement with the earlier reports.[24]

Photoluminescence (PL) measurement is a sensitive non-destructive technique to investigate the intrinsic and extrinsic defects in a semiconductor. It provides abundant information on the energy states of impurities and defects, even at very low densities, which is helpful for understanding structural defects in semiconductors. [25] The room temperature photoluminescence of

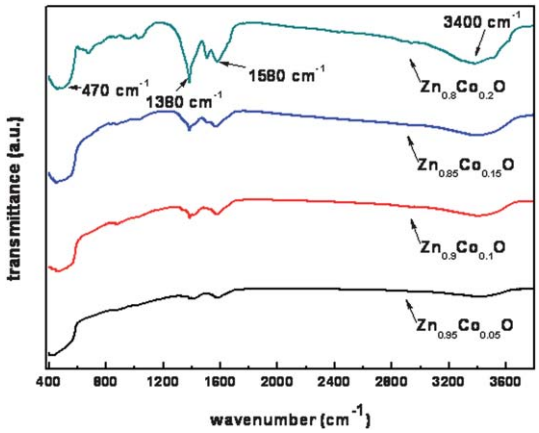

Fig. 5 FTIR spectra of $Zn_{1-x}Co_xO$ nanorods prepared by the solvothermal method.

$Zn_{1-x}Co_xO$ NRs is exhibited in Fig. 6, all samples exhibit a weak UV emission centered at near 402 nm, and a strong blue–green emission band (472–524 nm) (black lines). Meanwhile, the shift of the UV emission peaks to the longer wavelength side can be observed, which may be attributed to the strong exchange interactions between the "d" electrons of the doping ion and the "s" and "p" electrons of the host band. The existence of strong sp–d exchange interactions was confirmed by the observation of a strong magneto-optical effect near the band gap region of $Zn_{1-x}Co_xO$ alloys.[26]

In addition, there are three distinct emission peaks in the emission bands (black lines), the Gaussian model fitting results are also shown in Fig. 6 (color curves). The peaks at 472 nm and 495 nm belong to the blue emission, and that at 523 nm is green emission. Generally speaking, the blue and green emissions of ZnO are usually very weak and broad, particularly for the enhanced blue emission, which was infrequent in the previous reports. [27–29] However, in current work, an obvious blue–green enhanced emission in $Zn_{1-x}Co_xO$ NRs has been observed. Recent research has shown that surface defects are primarily responsible for the visible emission, [30–33] and the contribution of surface defects to visible emission can be reflected by the value of I_D/I_B (the ratio of defect- to near-bandgap emission). [30] Here, the calculated values of I_D/I_B are 2.96, 2.68, 2.03 and 1.53 for $Zn_{0.95}Co_{0.05}O$, $Zn_{0.9}Co_{0.1}O$, $Zn_{0.85}Co_{0.15}O$ and $Zn_{0.8}Co_{0.2}O$, respectively. These results indicate that Co^{2+} replacing Zn^{2+} leads to the quenching of visible light. The above results are further supported by the observed phenomenon that the intensity of blue–green emission bands decrease with the increase in Co^{2+}.

The UV emission is attributed to the radiative recombination of a hole in the valence band and an electron in the conduction band.[34,35] However, the origins of the visible luminescence from ZnO have been greatly controversial, especially for the blue emissions. It is generally accepted that the emissions in the visible regions are associated with the intrinsic or extrinsic defects in ZnO. Recently, Zeng *et al.*[36] reported that blue emission can be interpreted by the transition of extended Zn_i states. Here, as for the improvement of the blue–green emission band, we tend to the explanation that improvement in utilizing the efficiency of the exciting photons in the radiative recombination leads to the strong blue emission.[37] About the green emission, which can be

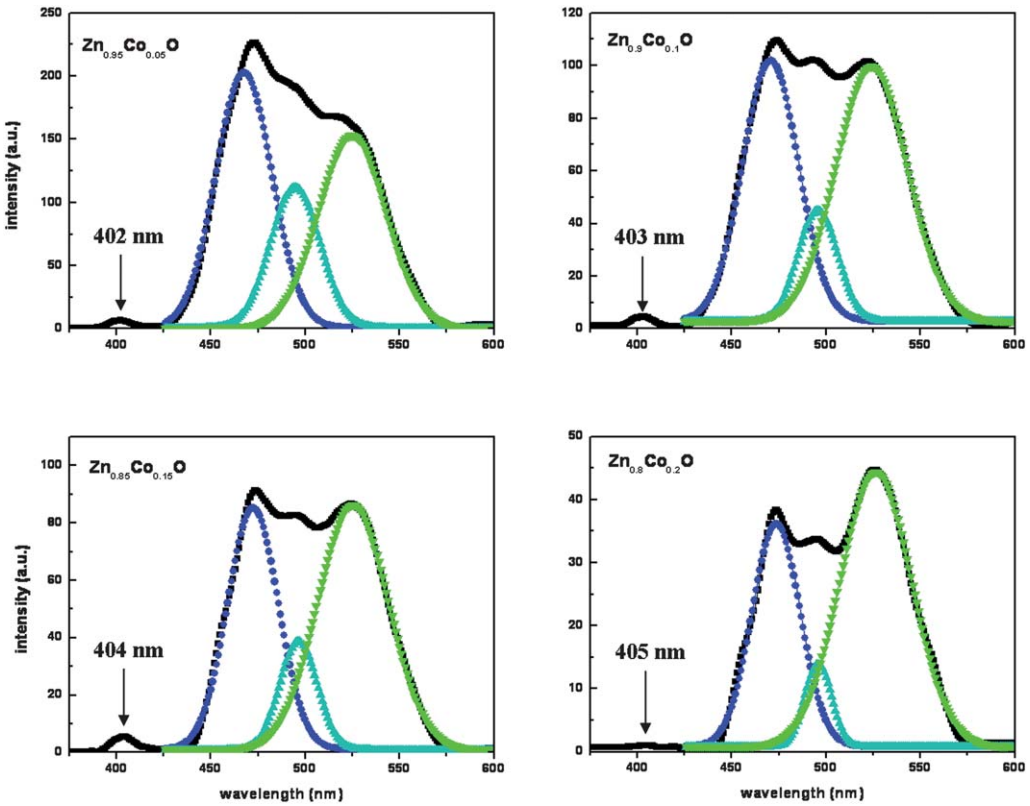

Fig. 6 Room-temperature PL spectra of $Zn_{1-x}Co_xO$ NRs (excitation light: xenon lamp; excitation wavelength: 325 nm).

ascribed to singly ionized oxygen vacancies in ZnO, it arises from the radiative recombination of a photogenerated hole with an electron occupying the oxygen vacancy.[38]

Optical absorption spectra of Co doped ZnO nanocrystals with varying dopant ion concentrations are presented in Fig. 7. Here, a distinct red shift is observed for the $Zn_{1-x}Co_xO$ nanocrystals, indicating that Co^{2+} in ZnO nanocrystals is able to tune the energy gap toward a low energy. The reduction of the energy gap caused by Co^{2+} doping in ZnO is a manifestation of the sp–d exchange interactions between the band electrons and the localized d electrons of the Co^{2+} ions substituting for Zn^{2+} ions.[39–42]

Co^{2+} ligand field absorption features [40] are clearly visible in Fig. 7, and the three characteristic absorption peaks are at 567, 611, and 652 nm, respectively. The phenomenon can be explained by cobalt-related $^4A^2$ (F)$\rightarrow{}^2A_1$ (G), $^4A_2$ (F)$\rightarrow{}^4T_1$ (P), and $^4A_2$ (F)$\rightarrow{}^2E$ (G) ligand field transitions for the tetrahedral symmetry of transition metal ions.[40] Absorption edges at around 620 nm are attributed to d–d transitions of Co^{2+} (d^7) in a tetrahedral coordination, as assigned to $^4A_2$ (F)$\rightarrow{}^4T_1$ (P), and $^4A_2$ (F)$\rightarrow{}^2E$ (G) ligand field transitions[40] suggesting that most Co ions are substituted for Zn sites in the host ZnO lattice. In brief, according to Hund's rule and Pauli's exclusion principle, the electronic ground-state configuration of a Co^{2+} ($3d^7$ configuration) has $L = 3$ and $S = 3/2$. So, the ground-state spectral term is ^4F and the excited state terms are ^4P, ^2G, ^2F, ^2D, and ^2P. However, when Co^{2+} exists in the tetrahedral field, the ^4F term splits into $^4A_2$ (F), $^4T_2$ (F), and $^4T_1$ (F), with $^4A_2$ (F) being lowest in energy and the remaining two having higher energies. The ^4P term corresponding to the first excited state does not split but is transformed into $^4T_1$ (P). Similarly, ^2G splits into $^2A_1$ (G), ^2E (G), $^2T_1$ (G), and $^2T_2$ (G). In the ground state, the atom is in the $^4A_2$ state. When the electron has sufficient energy, it can be excited to higher energy states.[43] The optical absorption study confirms the presence of high spin Co^{2+} (d^7) states in the ZnO lattice. Furthermore, the intensity of d–d transitions increases with the increase in number of Co^{2+} ions in ZnO nanocrystals.[44] The optical absorption measurements further verified that incorporation of Co^{2+} substitutes Zn^{2+} in ZnO nanocrystals.

Finally, the magnetic properties of $Zn_{1-x}Co_xO$ NRs with different Co doping contents from VSM measurements are

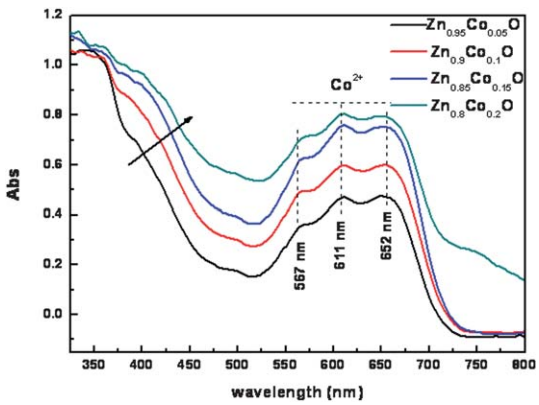

Fig. 7 Optical absorption spectra for $Zn_{1-x}Co_xO$ NRs.

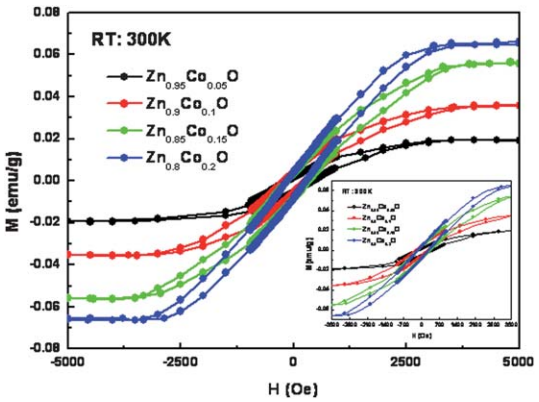

Fig. 8 Magnetization *versus* magnetic field (M–H) curves at room temperature (300 K) for $Zn_{1-x}Co_xO$ NRs; the inset shows the enlargement of the hysteresis loops near the origin.

shown in Fig. 8. All samples exhibit well-defined hysteresis loops at room temperature, indicating an obvious room-temperature ferromagnetic behavior. As shown in Fig. 8, the saturation magnetization (M_s) values of the four samples increase with cobalt doping content. However, M_s per cobalt decreases with increasing content of Co. Previously, similar results in diluted magnetic semiconductors (DMSs) have been reported.[38,45,46] Indirect interaction of Co^{2+} leads to ferromagnetism, whereas direct interaction of Co^{2+} can result in antiferromagnetism. With an increase in Co doping, the average distance between Co^{2+} decreases, leading to enhancement of the antiferromagnetic contribution.[46]

The origin of ferromagnetism in DMS materials has been controversial, while structural defects and magnetic impurities have often been used to explain magnetic ordering.[47–49] Besides, the magnetic behavior is highly dependent on the synthesis conditions.[50] Here, the room-temperature ferromagnetism of $Zn_{1-x}Co_xO$ NRs could originate from long range Co^{2+}–Co^{2+} ferromagnetic coupling mediated by itinerant electrons. Therefore, it can be concluded that the detected ferromagnetism arises from the homogeneous doping of Co^{2+} into the ZnO crystal lattice. However, the origin of the observed ferromagnetic behavior at room temperature needs to be further investigated.

Conclusion

In summary, 1D and high-quality single crystals of Co doped ZnO nanorods have been synthesized by a facile and low cost solvothermal approach. The nanorods are single crystals and the growth direction is the c-axis [0001] direction. It is found that the structural, optical and magnetic properties are sensitively dependent on the incorporation of Co^{2+} ions in the Zn^{2+} lattice site. The subsequent XRD, XPS, EDS, HRTEM and UV-vis spectroscopic characterization confirm that Co has successfully been doped into the lattice of ZnO. The doping of Co^{2+} ions can improve the blue–green emission, and we believe that the enhanced blue–green emission may be due to improvement in utilizing the efficiency of the exciting photons in radiative recombination. The UV emission shows a red shift with increasing Co^{2+}, which indicates a shift in the band gap to the lower-energy side. In addition, the magnetic measurement indicates that the $Zn_{1-x}Co_xO$ NRs have obvious ferromagnetic characteristics at room temperature, and the detected ferromagnetism could arise from the homogeneous doping of Co^{2+} into the ZnO crystal lattice. With this study we move one step closer toward controlling the properties of ZnO NRs, which would be very significant for applications in devices.

Acknowledgements

The work is supported by the National Science Foundation of China (51072001, 11174002, and 51102072), Anhui Provincial Key Laboratory of Information Materials and Devices, the Anhui Provincial Natural Science Fund (090414177), Anhui University "211" Engineering (06130221). Besides, the authors thank Prof. Huizhong Kou (Department of Chemistry, Tsinghua University) and Prof. Gang He for their valuable help.

References

1 D. J. Norris, A. L. Efros and S. C. Erwin, *Science*, 2008, **319**, 1776.
2 D. Mocatta, G. Cohen, J. Schattner, O. Millo, E. Rabani and U. Banin, *Science*, 2011, **332**, 77.
3 U. Ozgur, Y. I. Alivov, C. Liu, A. Teke, M. A. Reshchikov, S. D. ogan, V. Avrutin, S. J. Cho and H. J. Morkoc, *J. Appl. Phys.*, 2005, **98**, 041301.
4 T. Dietl, H. Ohno, F. Matsukura, J. Cibert and D. Ferrand, *Science*, 2000, **287**, 1019.
5 S. A. Wolf, D. D. Awschalom, R. A. Buhrman, J. M. Daughton, S. von Molnaár, M. L. Roukes, A. Y. Chtchelkanova and D. M. Treger, *Science*, 2001, **294**, 1488.
6 B. Panigrahy, M. Aslam, D. S. Misra, M. Ghosh and D. Bahadur, *Adv. Funct. Mater.*, 2010, **20**, 1161.
7 Y. C. Choi, W. S. Kim, Y. S. Park, S. M. Lee, D. J. Bae, Y. H. Lee, G. S. Park, W. B. Choi, N. S. Lee and J. M. Kim, *Adv. Mater.*, 2000, **12**, 746.
8 J. H. Choi, H. Tabata and T. J. Kawai, *J. Cryst. Growth*, 2001, **226**, 493.
9 M. Huang, Y. Yu, H. Feick, N. Tran, E. Weber and P. Yang, *Adv. Mater.*, 2001, **13**, 113.
10 Y. Li, G. W. Meng, L. D. Zhang and F. Phillip, *Appl. Phys. Lett.*, 2000, **76**, 2011.
11 B. Panigrahy, M. Aslam and D. Bahadur, *J. Phys. Chem. C*, 2010, **114**, 11758.
12 S. K. Mandal, A. K. Das, T. K. Nath and D. Karmakar, *Appl. Phys. Lett.*, 2006, **89**, 144105.
13 T. Fukamura, Z. Jin, A. Ohtomo, H. Koinuma and M. Kawasaki, *Appl. Phys. Lett.*, 1999, **75**, 3366.
14 J. Zhang, R. Skomski and D. J. Sellmyer, *J. Appl. Phys.*, 2005, **97**, 303.
15 R. Viswanatha, S. Sapra, S. S. Gupta, B. Satpati, P. V. Satyam, B. N. Dev and D. D. Sarma, *J. Phys. Chem. B*, 2004, **108**, 6303.
16 X. F. Wang, J. B. Xu, X. J. Yu and K. Xue, *Appl. Phys. Lett.*, 2007, **91**, 031908.
17 R. D. Shannon, *Acta Crystallogr., Sect. A: Cryst. Phys., Diffr., Theor. Gen. Crystallogr.*, 1976, **32**, 751.
18 B. J. Tan, K. J. Klabunde and P. M. A. Sherwood, *J. Am. Chem. Soc.*, 1991, **113**, 855–861.
19 K. X. Yao and H. C. Zeng, *J. Phys. Chem. C*, 2009, **113**, 1373.
20 J. W. Quilty, A. Shibata, J. Y. Son, K. Takubo, T. Mizokawa, H. Toyosaki, T. Fukumura and M. Kawasaki, *Phys. Rev. Lett.*, 2006, **96**, 027202.
21 G. B. Deacon and R. J. Philips, *Coord. Chem. Rev.*, 1980, **33**, 227.
22 F. Luo, L. D. Wang, B. B. Ma and Y. Qiu, *J. Photochem. Photobiol., A*, 2008, **197**, 378.
23 K. Kilsa, E. I. Mayo, B. S. Brunschwig, H. B. Gray, N. S. Lewis and J. R. Winkler, *J. Phys. Chem. B*, 2004, **108**, 15640.
24 M. Bitenc, G. Dražić and Z. C. Orel, *Cryst. Growth Des.*, 2010, **10**, 830.

25 J. Li, H. Q. Fan, X. H. Jia, W. W. Yang and P. Y. Fang, *Appl. Phys. A: Mater. Sci. Process.*, 2010, **98**, 537.
26 K. Ando, H. Saito, Z. Jin, T. Fukumura, M. Kawasaki, Y. Matsumoto and H. Koinuma, *Appl. Phys. Lett.*, 2001, **78**, 2700.
27 J. J. Wu and S. C. Liu, *Adv. Mater.*, 2002, **14**, 215.
28 W. H. Zhang, J. L. Shi, L. Z. Wang and D. S. Yan, *Chem. Mater.*, 2000, **12**, 1408.
29 L. Guo, S. H. Yang, C. L. Yang, P. Yu, J. N. Wang, W. K. Ge and G. K. L. Wong, *Chem. Mater.*, 2000, **12**, 2268.
30 J. V. Foreman, J. Li, H. Y. Peng, S. J. Choi, H. O. Everitt and J. Liu, *Nano Lett.*, 2006, **6**, 6.
31 D. Li, Y. H. Leung, A. B. Djurisic, Z. T. Liu, M. H. Xie, S. L. Shi, S. J. Xu and W. K. Chan, *Appl. Phys. Lett.*, 2004, **85**, 1601.
32 A. B. Djurisic, Y. H. Leung, W. C. H. Choy, K. W. Cheah and W. K. Chan, *Appl. Phys. Lett.*, 2004, **84**, 2635.
33 I. Shalish, H. Temkin and V. Narayanamurti, *Phys. Rev. B: Condens. Matter Mater. Phys.*, 2004, **69**, 245401.
34 J. J. Wu, H. I. Wen, C. H. Tseng and S. C. Liu, *Adv. Funct. Mater.*, 2004, **14**, 806.
35 B. Panigrahy, M. Aslam, D. S. Misra and D. Bahadur, *CrystEngComm*, 2009, **11**, 1920.
36 H. B. Zeng, G. T. Duan, Y. Li, S. K. Yang, X. X. Xu and W. P. Cai, *Adv. Funct. Mater.*, 2010, **20**, 561.
37 H. B. Zeng, W. P. Cai, P. S. Liu, X. X. Xu, H. J. Zhou, Claus Klingshirn and Heinz Kal, *ACS Nano*, 2008, **2**, 1661.
38 Y. C. Qiu, W. Chen, S. H. Yang, B. Zhang, X. X. Zhang, Y. C. Zhong and K. S. Wong, *Cryst. Growth Des.*, 2010, **10**, 177.
39 D. Y. Inamdar, A. D. Lad, A. K. Pathak, I. Dubenko, N. Ali and S. Mahamuni, *J. Phys. Chem. C*, 2010, **114**, 1451.
40 P. Koidl, *Phys. Rev. B: Solid State*, 1977, **15**, 2493.
41 Y. Z. Yoo, T. Fukumura, Z. Jin, K. Hasegawa, M. Kawasaki, P. Ahmet, T. Chikyow and H. Koinuma, *J. Appl. Phys.*, 2001, **90**, 4246.
42 S. Deka and P. A. Joy, *Appl. Phys. Lett.*, 2006, **89**, 032508.
43 A. Singhal, S. N. Achary, J. Manjanna, S. Chatterjee, P. Ayyub and A. K. Tyagi, *J. Phys. Chem. C*, 2010, **114**, 3422.
44 M. Gaudon, O. Toulemonde and A. Demourgues, *Inorg. Chem.*, 2007, **46**, 10996.
45 M. Venkatesan, C. B. Fitzgerald, J. G. Lunney and J. M. D. Coey, *Phys. Rev. Lett.*, 2004, **93**, 177206.
46 J. L. MacManus-Driscoll, N. Khare, Y. Liu and M. E. Vickers, *Adv. Mater.*, 2007, **19**, 2925.
47 K. C. Barick, M. Aslam, V. P. Dravid and D. Bahadur, *J. Phys. Chem. C*, 2008, **112**, 15163.
48 A. Sundaresan, R. Bhargavi, N. Rangarajan, U. Siddesh and C. N. R. Rao, *Phys. Rev. B: Condens. Matter Mater. Phys.*, 2006, **74**, 161306(R).
49 J. B. Yi, H. Pan, J. Y. Lin, J. Ding, Y. P. Feng, S. Thongmee, T. Liu, H. Gong and L. Wang, *Adv. Mater.*, 2008, **20**, 1170.
50 G. Clavel, M. G. Willinger, D. Zitoun and N. Pinna, *Adv. Funct. Mater.*, 2007, **17**, 3159.

